Communication

Observation of the TWIP + TRIP Plasticity-Enhancement Mechanism in Al-Added 6 Wt Pct Medium Mn Steel

SEAWOONG LEE, KYOOYOUNG LEE, and BRUNO C. DE COOMAN

The intercritically annealed Fe-0.15 pctC-6.0 pctMn-1.5 pctSi-3.0 pctAl and Fe-0.30 pctC-6.0 pctMn-1.5 pctSi-3.0 pctAl medium Mn steels were found to have improved mechanical properties due to the TWIP and TRIP plasticity-enhancing mechanisms being activated in succession during tensile deformation. The increase of the C content from 0.15 to 0.30 pct resulted in ultra-high strength properties and a strength-ductility balance of approximately 65,000 MPa-pct, *i.e.*, equivalent to the strength-ductility balance of high Mn TWIP steel with a fully austenitic microstructure.

DOI: 10.1007/s11661-015-2854-z

There is an increasing interest in medium Mn steel, and it is widely thought that this class of ferrous alloys could be used for the production of the body-in-white of passenger cars. Their ultra-fine-grained (UFG) microstructure is obtained by a relatively simple intercritical annealing process.[1–4] Due to a combination of grain size refinement and partitioning effects, a large volume fraction of UFG austenite can be stabilized at room temperature. This results in a superior combination of an ultra-high ultimate tensile strength and an exceptionally large uniform elongation due to the occurrence of the plasticity-enhancing deformation-induced martensitic transformation. The present contribution reports that a considerable enhancement of these properties was achieved in the course of the development of Al-added 6 wt pct medium Mn steel.

The occurrence of localized deformation currently limits the industrial use of UFG medium Mn steel. Hu[5] reported a Hall–Petch-type relation between the Lüders strain and the grain size. He also observed that the Lüders strain increased with decreasing grain size. According to Fujita and Miyazaki,[6] localized deformation is an unavoidable problem in fine-grained microstructures. Estrin and Kubin[7] argued that Lüders-type deformation resulted from the low work hardening rate of fine-grained materials, and that a localized Lüders-type deformation could only be reduced or eliminated by increasing the work hardening rate. The following methods increase the work hardening rate by enhancing dislocation storage during deformation: (a) the use of a dual phase microstructure, (b) the introduction of precipitates in the microstructure, (c) the activation of a plasticity-enhancing phase transformation, (d) the use of a microstructure with a bimodal grain size distribution, and (e) the formation of mechanical twins during straining.

Medium Mn steel contains a large volume fraction of intercritical austenite stabilized at room temperature as a result of grain size refinement and the partitioning of C and Mn to the intercritical austenite.[2,3] Lee *et al.*[8] showed that the strain-induced martensitic transformation resulted in a transformation-induced plasticity (TRIP) effect which drastically increased the work hardening rate in uniaxial tensile testing. They also showed that the localized deformation in medium Mn steel could be eliminated by Al-additions which resulted in the presence of coarse-grained δ-ferrite in the microstructure. Allain *et al.*[9] showed that when the stacking fault energy (SFE) of fully austenitic twinning-induced plasticity (TWIP) steel was in the range of 20 to 50 mJ/m^2, a high work hardening rate was obtained from deformation-induced twinning. The mechanical twinning was suppressed at higher SFE values. Deformation-induced martensitic transformation occurred when the SFE was lower than 18 mJ/m^2. Recently, Lee *et al.*[10] showed that the combination of mechanical twinning and strain-induced martensitic transformation increased the work hardening rate considerably and resulted in an exceptional improvement of the mechanical properties in a 10 pct Mn steel. In the present study, the design of Al-added medium Mn steel was done by means of an intercritical annealing temperature diagram which allows for the determination of the effect of the intercritical annealing temperature on the mechanical properties. The approach resulted in the development of intercritically annealed medium Mn steel which had improved mechanical properties due to the TWIP and TRIP plasticity-enhancing mechanisms being activated in succession during tensile deformation.

The chemical compositions of the two steels studied in the present work were Fe-0.15 pctC-6.0 pctMn-1.5 pctSi-3.0 pctAl and Fe-0.30 pctC-6.0 pctMn-1.5 pctSi-3.0 pctAl (in mass pct). Ingots with a thickness of 100 mm were prepared by vacuum induction melting, reheated to 1523 K (1250 °C), hot rolled to a thickness of 3 mm and cooled in the air. The hot-rolled strip was cold rolled to a thickness of 1 mm. The cold-rolled steel was intercritically annealed in a continuous annealing simulator under a protective N_2 gas atmosphere. The heating rate was + 3 °C/s, the holding time at the intercritical soaking temperature was 180 seconds, and the cooling to room temperature was done with a cooling rate of −30 °C/s.

SEAWOONG LEE, Graduate Student, is with the Graduate Institute of Ferrous Metallurgy, Pohang University of Science and Technology (POSTECH), Pohang, South Korea. KYOOYOUNG LEE, Senior Researcher, is with the POSCO Technical Research Laboratories, Gwangyang, South Korea. BRUNO C. DE COOMAN, Professor, is with the Graduate Institute of Ferrous Metallurgy, Pohang University of Science and Technology (POSTECH) and also Director with the Materials Design Laboratory, Pohang University of Science and Technology, Pohang, South Korea. Contact e-mail: decooman@postech.ac.kr

Manuscript submitted December 23, 2014.
Article published online March 21, 2015

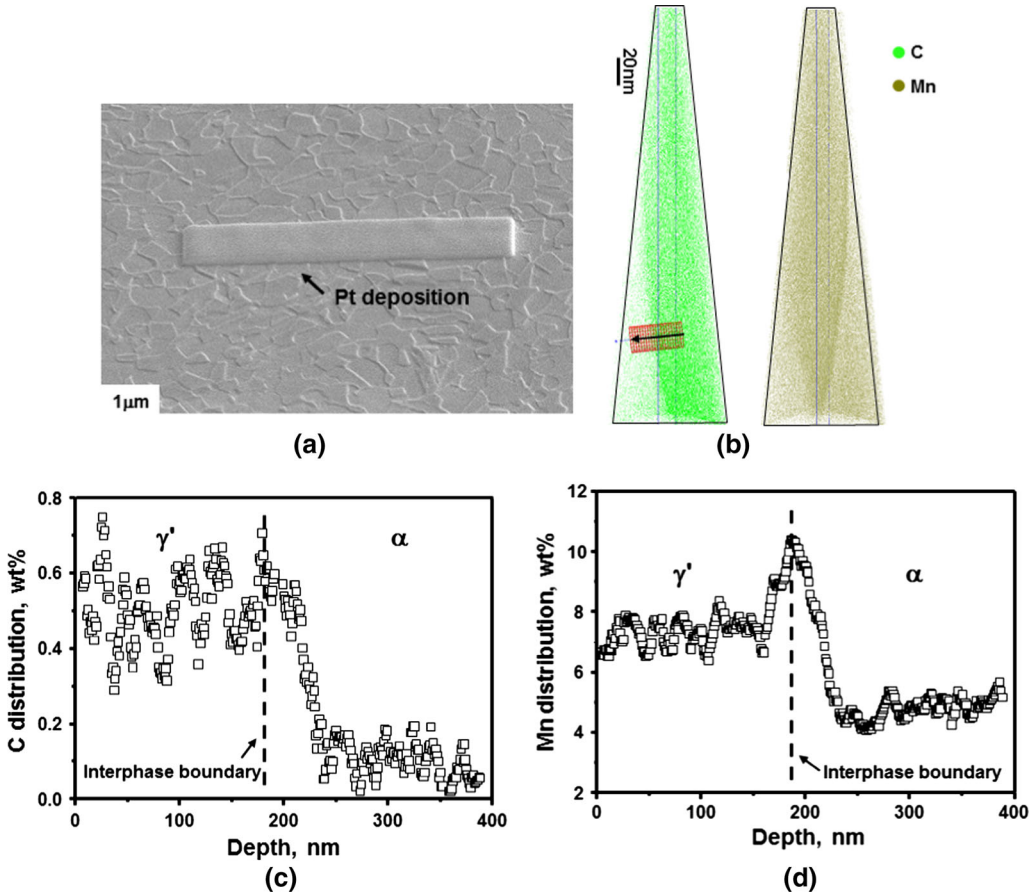

Fig. 1—3D Atom Probe (AP) tomography for Fe-0.15 pctC-6.0 pctMn-1.5 pctSi-3.0 pctAl steel intercritically annealed at 1113 K (840 °C). (*a*) FE-SEM micrograph showing the ultra-fine-grained two phase microstructure selected for 3D atom probe analysis. (*b*) C and Mn distribution in the 3D atom probe sample. (*c*) C concentration profile across the ferrite/austenite interface in the area indicated in (b). (*d*) Mn concentration profile across the ferrite/austenite interface in the area indicated in (b).

Three-dimensional atom probe (3D AP) tomography was carried out in a CAMECA laser-assisted wide-angle tomographic atom probe equipped with a 343 nm Ultra-Violet femtosecond-pulse laser. The 3D AP samples were made by means of the Focused-Ion-Beam technique.

Rectangular dilatometric specimens, 1 mm × 5 mm × 10 mm in size, machined from cold-rolled sheet and intercritically annealed at a temperature in the range of 973 K to 1173 K (700 °C to 900 °C), were used to measure the room temperature volume fraction of austenite by means of the magnetic saturation method.

ASTM-E8 standard samples, with their length aligned parallel to the rolling direction, were uni-axially tested in tension up to fracture using a strain rate of 10^{-3} s^{-1} in a ZWICK Z100 universal tensile testing machine.

Transmission electron microscopy (TEM) observations were carried on tensile samples after tensile deformation to identify the deformation mechanisms, using a JEOL 2100F TEM equipped with a field-emission source operated at an accelerating voltage of 200 kV. Thin foil TEM specimens were prepared by twin jet electro-polishing 3-mm diameter disks using a solution of 10 pct perchloric acid and 90 pct acetic acid. In addition, a nano-beam size energy dispersive spectroscopy (EDS) system was used to analyze the composition of the microstructural constituents.

Figure 1 shows 3D AP results from intercritically annealed Fe-0.15 pctC-6.0 pctMn-1.5 pctSi-3.0 pctAl steel. Figure 1(a) shows a micrograph of the microstructure after intercritical annealing at 1113 K (840 °C) for 180 seconds prior to 3D AP sample extraction. The micrograph shows the UFG area with the Pt deposit which was ion-milled to obtain a needle type sample. Figure 1(b) shows the C and Mn distribution across a ferrite and austenite grain. The phase boundary was approximately parallel to the length of the 3D AP sample. There is a clear difference in the C and Mn content in the ferrite and austenite. Figure 1(b) shows that there is a large C enrichment in austenite, and that C was depleted in the ferrite phase. The Mn distribution is shown in the Figure 1(d). The partitioning of Mn between ferrite and austenite is also clearly visible. In addition, a Mn segregation peak up to 10 wt pct Mn was observed along the interphase boundary. Enomoto reported[11] that the large discrepancy between the calculated and the experimental growth rate of ferrite during the austenite-to-ferrite transformation originated from a solute drag effect due to Mn atoms, segregated at the ferrite/austenite phase boundary. It appears that in the present case, the UFG structure of the

6 wt pct medium Mn steel could be obtained at high annealing temperature due to a Mn solute drag effect at the interphase boundary which reduced the interphase mobility, thereby stabilizing the UFG microstructure.

Lee *et al.*[12] proposed a method to determine the optimal intercritical annealing temperature for UFG medium Mn steel. They defined the T_M temperature as the intercritical annealing temperature which resulted in the largest room temperature austenite volume fraction in the microstructure. They showed that optimal mechanical properties, *i.e.*, a combination of high strength and large ductility, were obtained when the steel was intercritically annealed at a temperature slightly lower than the T_M temperature. Figure 2 shows the application of this approach to the selection of the intercritical annealing temperature of Fe-0.15 pctC-6.0 pctMn-1.5 pctSi-3.0 pctAl steel. The original diagram was complemented with the annealing temperature dependence of the room temperature SFE of the UFG austenite.[13] The SFE calculation takes into account the higher amount of C and Mn in the intercritical austenite. The figure shows that the elemental partitioning leads to an increase in the room temperature SFE, which can result in the activation of mechanical twinning during deformation. The equilibrium Mn, Si, and Al contents in austenite were used to calculate the SFE

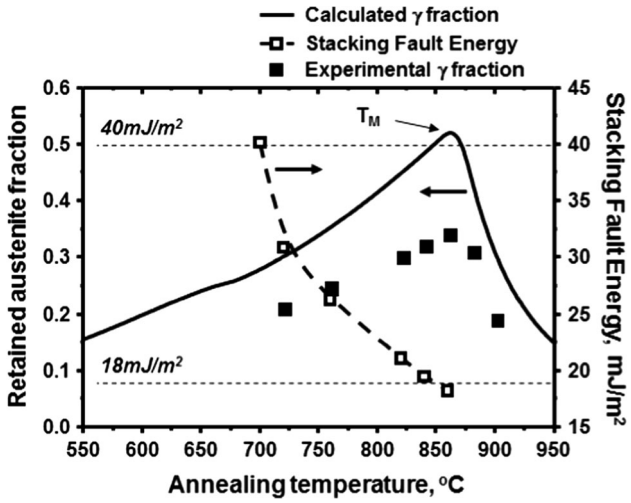

Fig. 2—Intercritical annealing temperature diagram for Fe-0.15 pctC-6.0 pctMn-1.5 pctSi-3.0 pctAl steel. The full line is the calculated annealing temperature dependence of the room temperature austenite volume fraction. The dotted line is the annealing temperature dependence of the room temperature SFE of the intercritical austenite. The full squares are experimentally measured room temperature austenite volume fractions.

as the Mn, Si, and Al contents have been shown to be close to their equilibrium value even after relatively short intercritical annealing times.[14] The C content was calculated assuming that the solubility of C in ferrite was negligible, *i.e.*, the austenite C content was set equal to the nominal alloy C content divided by the volume fraction of retained austenite. The composition of the UFG ferrite and austenite, as obtained from 3D AP measurements of the Fe-0.15 pctC-6.0 pctMn-1.5 pctSi-3.0 pctAl steel annealed at 1113 K (840 °C) for 180 seconds, is listed in Table I along with the composition obtained from equilibrium calculations. The use of equilibrium composition of the intercritical austenite to calculate the room temperature SFE is a valid working assumption as the compositions obtained from the 3D AP experiment were close to those obtained from equilibrium calculation. The measured C content of the UFG austenite was also close to the value obtained by assuming a negligible C solubility in ferrite at the intercritical annealing temperature. The austenite volume fractions obtained after intercritical annealing were always slightly lower than the calculated volume fraction as a result of short intercritical annealing times. It has previously been shown by Lee *et al.*[12] that the equilibrium austenite volume fraction could be obtained if the annealing time was sufficiently long. The selection of the optimal intercritical annealing temperature was done by considering both the T_M temperature and the room temperature SFE of the UFG austenite. An intercritical annealing temperature of 1113 K (840 °C) was selected as the corresponding room temperature SFE of the intercritical austenite was calculated to be about 20 mJ/m^2. This SFE value is known to result in mechanical twinning in high Mn TWIP steel with a fully austenitic microstructure. The approach is also in agreement with the selection of an optimal temperature slightly lower than the T_M temperature, as discussed previously by Lee *et al.*[12] An intercritical annealing treatment at 993 K (720 °C) was also carried out in order to compare the mechanical properties of medium Mn steel in which the UFG austenite has a SFE higher than 30 mJ/m^2.

Figure 3 shows the mechanical properties of the Fe-0.15 pctC-6.0 pctMn-1.5 pctSi-3.0 pctAl steel after an intercritical annealing at 993 K and 1113 K (720 °C and 840 °C). The corresponding volume fraction of the UFG austenite before and after tensile testing is listed in Table II. The UFG austenite in the steel annealed at 993 K (720 °C) did not undergo deformation-induced martensite transformation. On the other hand, a large volume fraction of the UFG austenite was transformed to martensite during the tensile deformation of the steel

Table I. Composition Obtained by 3D Atom Probe Tomography of the UFG Ferrite and Austenite in Fe-0.15 pctC-6.0 pctMn-1.5 pctSi-3.0 pctAl Steel After Intercritical Annealing at 1113 K (840 °C) for 180 s

Phase	C (Wt Pct)	Mn (Wt Pct)	Si (Wt Pct)	Al (Wt Pct)
Ferrite (α)	0.01 (0.008)	4.88 (4.36)	1.52 (1.40)	1.71 (3.48)
Austenite (γ)	0.48 (0.470)	6.55 (7.80)	1.19 (1.61)	1.33 (2.47)

The equilibrium compositions obtained by ThermoCalc® are given in parenthesis.

which was intercritically annealed at 1113 K (840 °C). As shown in the Figure 3, the steel intercritically annealed at 1113 K (840 °C) had clearly superior mechanical properties as compared to the same steel intercritically annealed at 993 K (720 °C), in terms of both strength and ductility. The mechanical properties of the steel after an intercritical annealing at 993 K and 1113 K (720 °C and 840 °C) are listed in Table III.

Figure 4 shows TEM micrographs of the medium steel annealed at 993 K (720 °C) after tensile testing. Both UFG austenite grains were free of planar faults (Figure 4(a)) and faulted (Figure 4(b)) UFG austenite grains were observed. No evidence of mechanical twinning or deformation-induced martensite formation was observed. The absence of mechanical twinning is due to the high room temperature SFE (30 mJ/m^2). The increased austenite stability, due to a combination of an ultra-fine grain size of approximately 250 nm, and a high C content of about 0.7 wt pct suppressed the deformation-induced martensitic transformation. The work hardening of Fe-0.15 pctC-6.0 pctMn-1.5 pctSi-3.0 pctAl was therefore relatively limited after an intercritical annealing at 993 K (720 °C).

Figure 5(a) compares the mechanical properties of the Fe-0.15 pctC-6.0 pctMn-1.5 pctSi-3.0 pctAl steel with

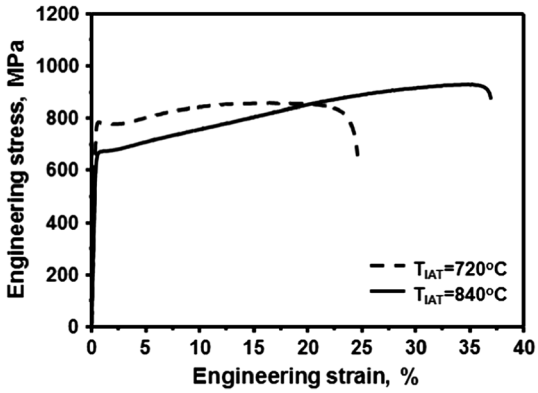

Fig. 3—Stress-strain curve of Fe-0.15 pctC-6.0 pctMn-1.5 pctSi-3.0 pctAl steel intercritically annealed at 993 K and 1113 K (720 °C and 840 °C).

those reported previously for similar medium Mn steels by Lee *et al.*[8,15] The figure shows that the Fe-0.05 pctC-6.15 pctMn-1.5 pctSi steel, intercritically annealed at 913 K (640 °C), displayed a Lüders-type localized deformation during tensile testing due to its UFG microstructure which is known to result in the suppression of strain hardening and the absence of a compensating plasticity-enhancing mechanism, such as deformation-induced martensite formation. In contrast, the Fe-0.08 pctC-6.0 pctMn-1.5 pctSi-2.0 pctAl-0.08 pctV steel intercritically annealed at 1013 K (740 °C) had a continuous yielding behavior and a high work hardening rate. The Fe-0.15 pctC-6.0 pctMn-1.5 pctSi-3.0 pctAl steel intercritically annealed at 1113 K (840 °C) showed a clear improvement of the mechanical properties particularly in terms of ductility. The improved mechanical properties in this steel were due to the introduction of two plasticity-enhancing mechanisms: (1) a microstructure containing coarse grained δ-ferrite and (2) the activation of the deformation-induced martensitic transformation. It was also shown in Reference 8 that the presence of the δ-ferrite, brought about by an increase of the Al content, effectively increased the work hardening rate in the early stages of tensile straining, thereby lowering the risk of localized deformation.

TEM micrographs taken from UFG austenite grains in the Fe-0.15 pctC-6.0 pctMn-1.5 pctSi-3.0 pctAl steel intercritically annealed at 1113 K (840 °C) are shown in Figure 6. The micrographs clearly illustrate that both mechanical twinning and deformation-induced martensitic transformation occurred in the UFG austenite grains. Figures 6(b) and (c) shows dark-field micrographs of the austenite matrix and mechanical twins. The twin reflections are clearly visible in the diffraction pattern. The Kurdjumov–Sachs orientation relationships ($\{111\}_\gamma//\{110\}_\alpha$, $\langle 110\rangle_\gamma//\langle 111\rangle_\alpha$) were observed between the UFG austenite and ferrite grains in Figure 6. As confirmed by the Mn distribution across the austenite/martensite interface in Figure 7(a), the constituent above the mechanically twinned UFG austenite grain was strain-induced martensite since its Mn content of 8.0 pct (Figure 7(d)) was higher than the

Table II. Volume Fraction of UFG Austenite in Fe-0.15 pctC-6.0 pctMn-1.5 pctSi-3.0 pctAl Steel Before and After Tensile Testing

Annealing Temperature [K (°C)]	Before Straining	After Straining	Transformed Volume Fraction
993 (720)	0.175	0.175	0.00
1113 (840)	0.281	0.098	0.18

Table III. Summary of the Mechanical Properties of Intercritically Annealed Fe-0.15 pctC-6.0 pctMn-1.5 pctSi-3.0 pctAl and Fe-0.3 pctC-6.0 pctMn-1.5 pctSi-3.0 pctAl Steel

Steel	Annealing Temperature [K (°C)]	Tensile Strength (MPa)	Total Elongation (pct)	UTS·TE MPa pct
Fe-0.15 pctC-6.0 pctMn-1.5 pctSi-3.0 pctAl	993 (720)	856	25	21,080
	1113 (840)	929	37	34,400
Fe-0.30 pctC-6.0 pctMn-1.5 pctSi-3.0 pctAl	1053 (780)	1131	58	65,360

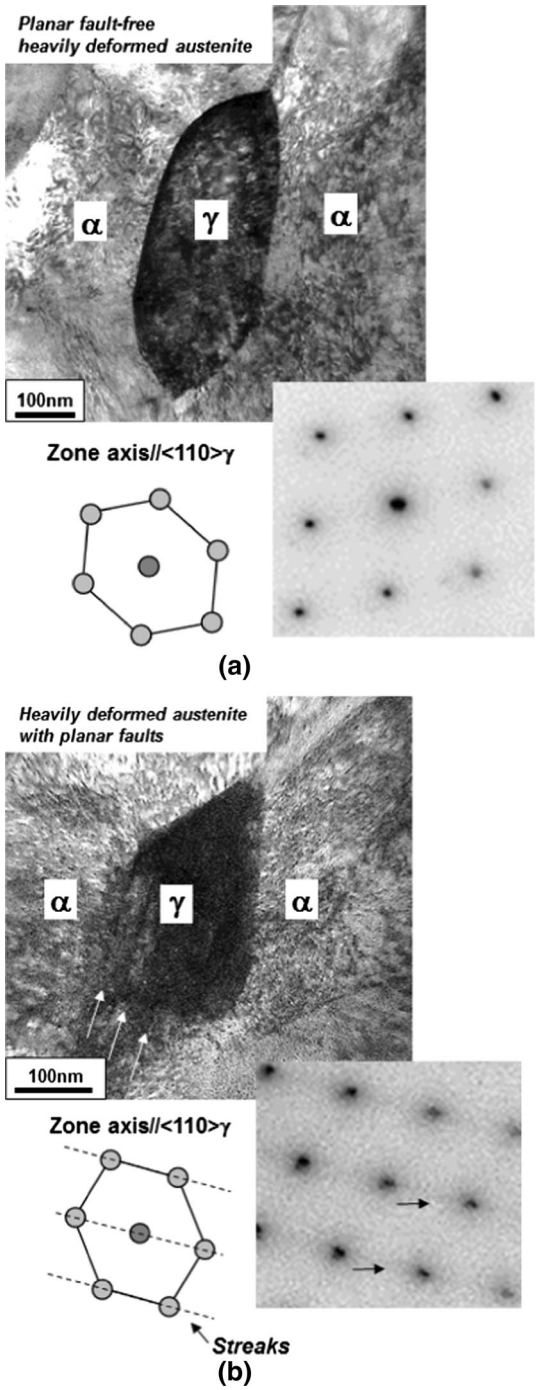

Fig. 4—Bright-field TEM micrograph of the UFG austenite in Fe-0.15 pctC-6.0 pctMn-1.5 pctSi-3.0 pctAl steel intercritically annealed at 993 K (720 °C) after tensile testing showing (*a*) an UFG austenite grain without planar faults, and (*b*) an UFG austenite grain with planar faults.

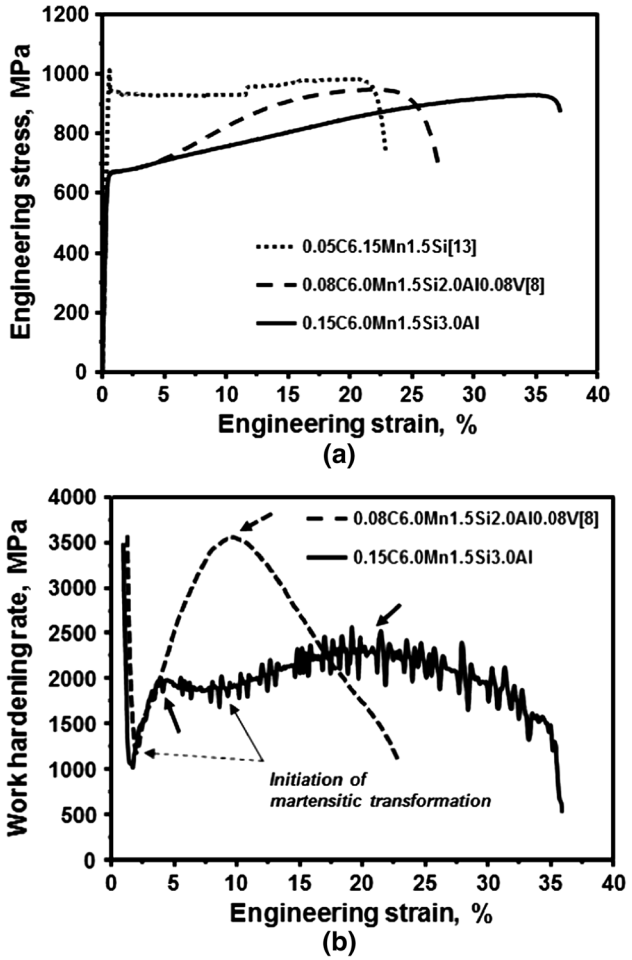

Fig. 5—(*a*) Comparison of the mechanical properties of three medium Mn steels. (*b*) Comparison of the work hardening of 0.08 pctC6 pctMn1.5 pctSi2.0 pctAl0.08 pctV steel (taken from Ref. [8]) and Fe-0.15 pctC-6.0 pctMn-1.5 pctSi-3.0 pctAl steel.

Mn content in the ferrite, which was approximately 4.8 pct (Table I) after intercritical annealing at 1113 K (840 °C). Lee *et al.*[10] have reported that mechanical twinning, followed by the strain-induced martensitic transformation as the twin formation reaches saturation, provided a powerful mechanism to increase the work hardening rate. They reported that the work hardening had two maxima, the first associated with deformation-induced twinning and the second due to strain-induced martensite nucleated at the twin–twin intersections.

Figure 5(b) shows the strain dependence of the work hardening for both of the Fe-6 pctMn-0.08 pctC-1.5 pctSi-2.0 pctAl-0.08 pctV steel[8] and Fe-0.15 pctC-6.0 pctMn-1.5 pctSi-3.0 pctAl steel, studied in the present work. The Fe-6 pctMn-0.08 pctC-1.5 pctSi-2.0 pctAl-0.08 pctV steel shows a continuous decrease in work hardening rate after reaching a maximum at 10 pct engineering strain. This implies that the work hardening is controlled by a single plasticity-enhancing mechanism, *i.e.*, the TRIP effect. No mechanical twinning was observed[8] because the room temperature SFE of the UFG austenite in the Fe-6 pctMn-0.08 pctC-1.5 pctSi-2.0 pctAl-0.08 pctV steel was only 7 mJ/m^2. A second strain hardening peak was, however, clearly observed for the Fe-0.15 pctC-6.0 pctMn-1.5 pctSi-3.0 pctAl steel. This is a typical feature of the strain hardening curve when two plasticity-enhancing mechanisms, in the present case the TWIP effect and the TRIP effect, occur in succession. The work hardening rate of

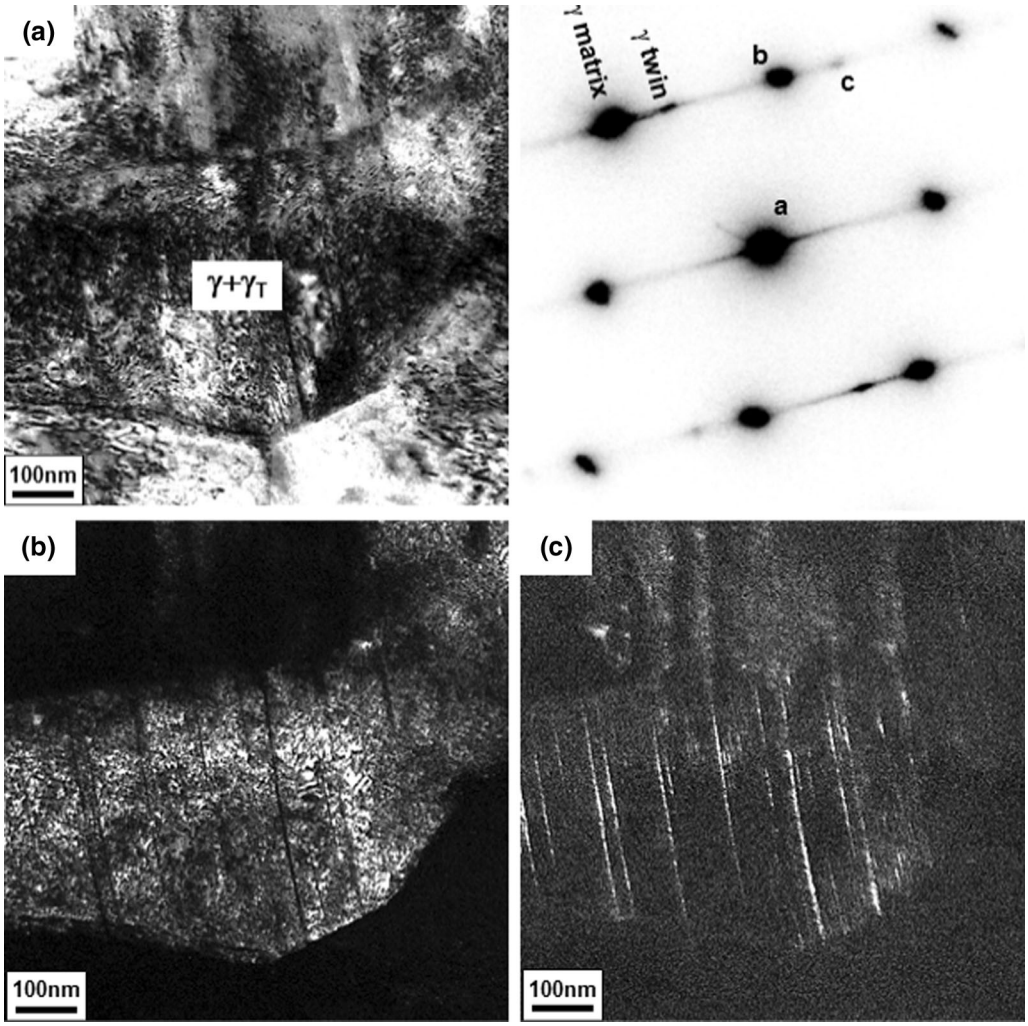

Fig. 6—TEM analysis of deformed UFG austenite in Fe-0.15 pctC-6.0 pctMn-1.5 pctSi-3.0 pctAl steel intercritically annealed at 1113 K (840 °C), showing mechanical twins formed during tensile testing. (*a*) Bright-field TEM micrograph of a twinned UFG austenite grain. (*b*) Corresponding dark-field TEM micrograph of the austenite matrix. (*c*) Corresponding dark-field TEM micrograph of the mechanical twins.

the Fe-0.15 pctC-6.0 pctMn-1.5 pctSi-3.0 pctAl steel decreased due to the saturation of the mechanical twinning at an engineering strain of approximately 10 pct. This was followed by the activation of the strain-induced martensitic transformation initiated at twin–twin intersections, which resulted in the upward slope of the work hardening rate until the work hardening rate reached a maximum at an engineering strain of approximately 22 pct, as shown in Figure 5(b).

The intercritical annealing temperature diagram for the Fe-0.3 pctC-6.0 pctMn-1.5 pctSi-3.0 pctAl steel is shown in Figure 8(a). The intercritical annealing temperature of 1053 K (780 °C) was selected by considering both of T_M temperature and room temperature SFE of the UFG austenite. After a 30 minutes intercritical annealing, an intercritical austenite volume fraction, close to equilibrium volume fraction, was obtained as shown in the Figure 8(a). Figure 8(b) compares the mechanical properties of the Fe-0.3 pctC-6.0 pctMn-1.5 pctSi-3.0 pctAl steel with those of the Fe-0.15 pctC-6.0 pctMn-1.5 pctSi-3.0 pctAl steel and two TWIP steels containing 18 pctMn and 15 pctMn, previously presented in Reference 16. Although the Fe-0.3 pctC-6.0 pctMn-1.5 pctSi-3.0 pctAl steel had considerably lower C and Mn contents, the steel had superior mechanical properties compared to those of the more highly alloyed, fully austenitic TWIP steel. In particular, the Fe-0.3 pctC-6.0 pctMn-1.5 pctSi-3.0 pctAl steel had a much higher yield strength due to its UFG microstructure as compared to TWIP steel. Figure 8(c) compares the work hardening rate of the TWIP steels and the Fe-0.3 pctC-6.0 pctMn-1.5 pctSi-3.0 pctAl Mn steel. The

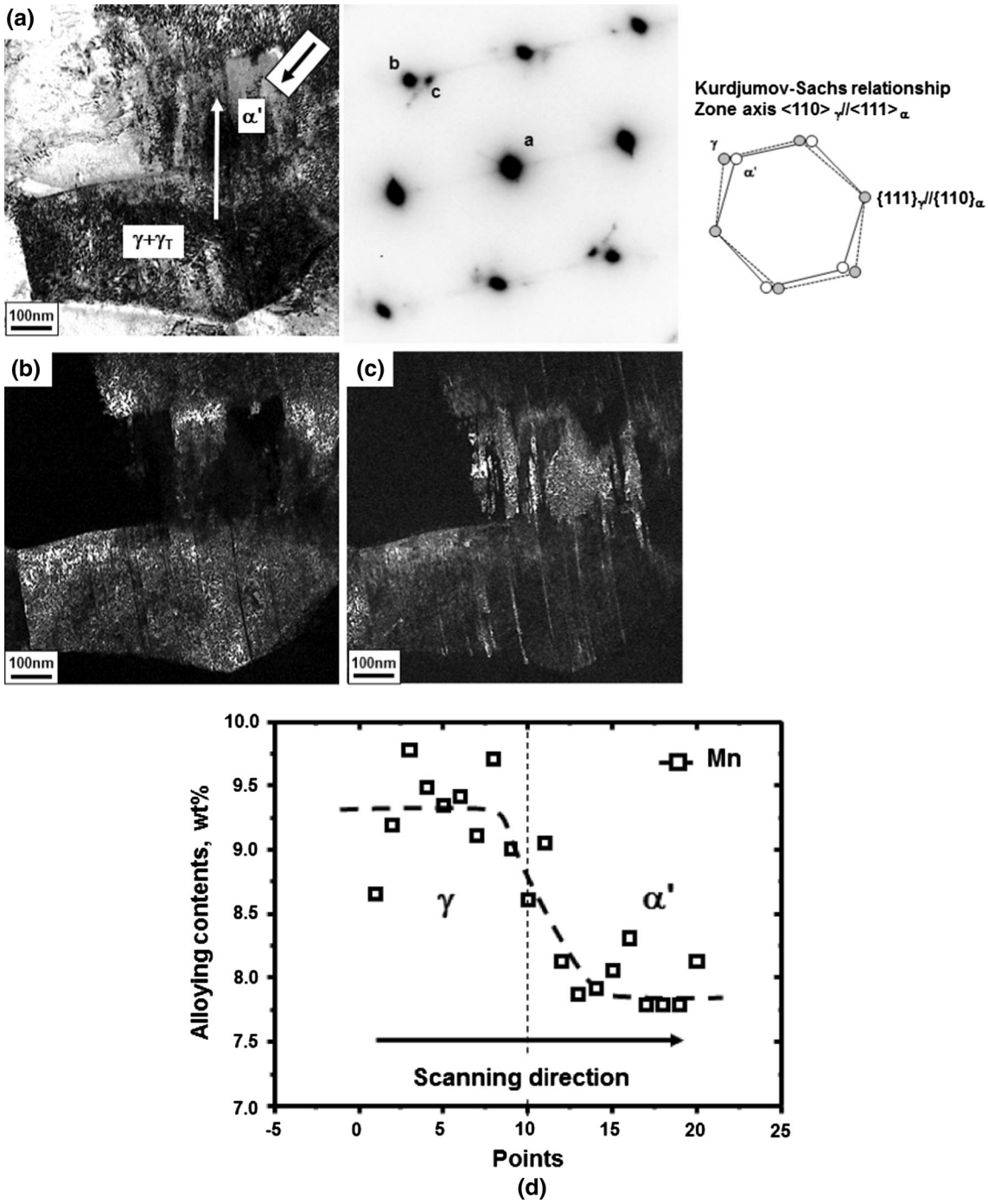

Fig. 7—TEM analysis of Fe-0.15 pctC-6.0 pctMn-1.5 pctSi-3.0 pctAl steel intercritically annealed at 1113 K (840 °C), showing the presence of strain-induced martensite formed during tensile testing. (*a*) Bright-field TEM micrograph of an austenite grain containing twins and strain-induced martensite. (*b*) Corresponding dark-field TEM micrograph of the austenite matrix. (*c*) Corresponding dark-field TEM micrograph of the twinned austenite and the strain-induced martensite. (*d*) Elemental Mn line profile obtained by STEM-EDS analysis along the white line indicated in (a).

combination of the TWIP effect and TRIP effect in succession is clearly visible, with the TRIP effect giving rise to a broad secondary peak in the strain hardening. Due to the higher C content of UFG austenite in the Fe-0.3 pctC-6.0 pctMn-1.5 pctSi-3.0 pctAl steel, it had an increased stability which resulted in a retardation of the initiation of deformation-induced martensitic transformation and reduction of martensitic transformation

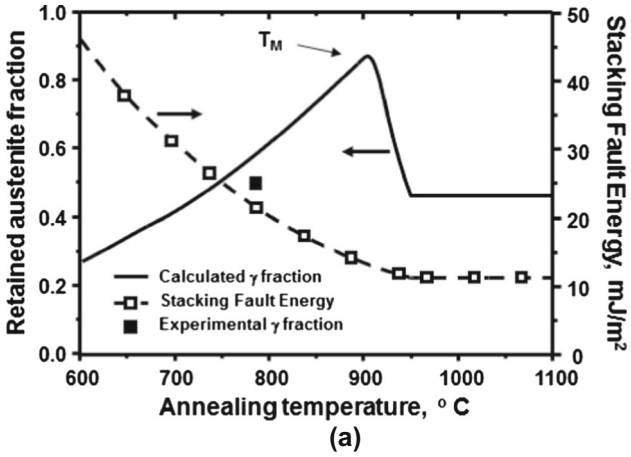

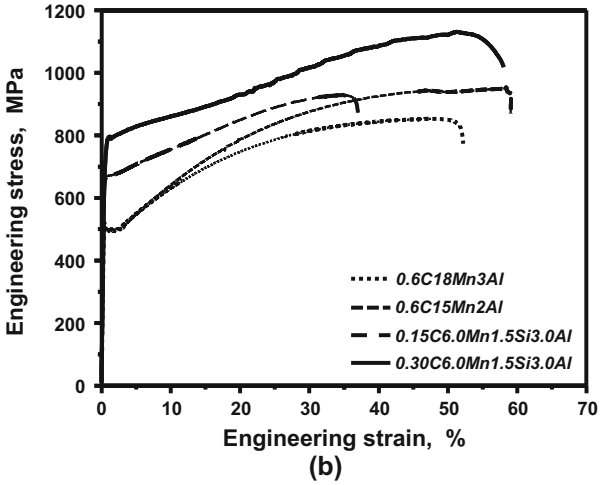

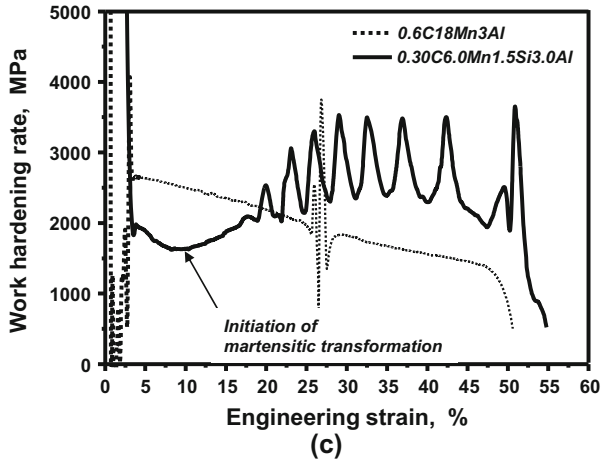

Fig. 8—(*a*) Intercritical annealing temperature diagram of the Fe-0.3 pctC-6.0 pctMn-1.5 pctSi-3.0 pctAl steel. The full line is the calculated annealing temperature dependence of the room temperature austenite volume fraction. The dotted line is the annealing temperature dependence of the room temperature SFE of the intercritical austenite. The full squares are experimentally measured room temperature austenite volume fractions. (*b*) Comparison of the mechanical properties of Fe-0.15 pctC-6.0 pctMn-1.5 pctSi-3.0 pctAl steel and Fe-0.3 pctC-6.0 pctMn-1.5 pctSi-3.0 pctAl steel, with the mechanical properties of high Mn, fully austenitic, TWIP steel. (*c*) Comparison of the work hardening rate of the Fe-0.6 pctC-18 pctMn-3.0 pctAl TWIP steel and the Fe-0.3 pctC-6.0 pctMn-1.5 pctSi-3.0 pctAl medium Mn steel.

kinetics.[3] This resulted in a higher ductility as compared to the Fe-0.15 pctC-6.0 pctMn-1.5 pctSi-3.0 pctAl steel. The work hardening of the fully austenitic Fe-0.6 pctC-18 pctMn-3.0 pctAl TWIP steel was consistent with only a single plasticity mechanism governing the work hardening.

In summary, it was found that the selection of the proper intercritical annealing temperature for Fe-0.15 pctC-6.0 pctMn-1.5 pctSi-3.0 pctAl and Fe-0.3 pctC-6.0 pctMn-1.5 pctSi-3.0 pctAl medium Mn steel, taking into consideration both the T_M temperature and the room temperature SFE of the austenite phase, resulted in exceptional mechanical properties. The annealing temperature should be slightly lower than the T_M temperature to take full advantage of a room temperature austenite SFE of approximately 20 mJ/m^2 to ensure mechanical twinning during deformation and deformation-induced martensitic transformation after the saturation of the TWIP effect. The activation of the TWIP and TRIP effects in succession lead to the mechanical properties for medium Mn steel which were comparable or better than those of fully austenitic high Mn TWIP steel.

The authors gratefully acknowledge Mr. Jonghan and Jae Hyuk Lee for their contribution to the 3D Atom Probe tomography experiments at the National Institute for Nanomaterials Technology (NINT), Pohang University of Science and Technology, South Korea.

REFERENCES

1. R.L. Miller: *Metall. Trans.*, 1972, vol. 3, p. 905.
2. H. Dong, W. Cao, J. Shi, C. Wang, M. Wang: *HMnS 2011 Conf. Proc.*, 2011, Seoul.
3. S. Lee, S.-J. Lee, S. Kumar, K. Lee, and B.C. De Cooman: *Metall. Mat. Trans. A*, 2011, vol. 42A, p. 3638.
4. Y.-U. Heo, Y.-Y. Song, S.-J. Park, H.K.D.H. Bhadeshia D.-W. Suh: *Metall. Mater. Trans. A*, 2012, vol. 43A, p. 1731.
5. H. Hu: *Metall. Trans. A*, 1983, vol. 14A, pp. 85–91.
6. H. Fujita and S. Miyazaki: *Acta Metall.*, 1978, vol. 26, pp. 1273–81.
7. Y. Estrin and L.P. Kubin: in *Continuum Models for Materials with Micro-structure*, H.E. Mülhaus, ed., Wiley, New York, 1995, p. 365.
8. S. Lee and B.C. De Cooman: *Metall. Mater. Trans. A*, 2013, vol. 44A, pp. 3136–46.
9. S. Allain, J.P. Chateau, D. Dahmoun, and O. Bouaziz: *Mater. Sci. Eng. A*, 2004, vols. 387–389, pp. 272–76.
10. S. Lee and B.C. De Cooman: *Metall. Mater. Trans. A*, 2014, vol. 45A, pp. 6039–52.
11. M. Enomoto: *Acta Mater.*, 1999, vol. 47, pp. 3533–40.
12. S. Lee and B.C. De Cooman: *Metall. Mater. Trans. A*, 2013, vol. 44A, pp. 5018–24.
13. A. Dumay, J.-P. Chateau, S. Allain, S. Migot, and O. Bouaziz: *Mater. Sci. Eng. A*, 2008, vols. 483–484, pp. 184–87.
14. S. Lee, S.-J. Lee, and B.C. De Cooman: *Scripta Mater.*, 2011, vol. 65, pp. 225–28.
15. S. Lee, S.-J. Lee, S. Santhosh Kumar, K. Lee, and B.C. De Cooman: *Metall. Mater. Trans. A*, 2011, vol. 42A, pp. 3638–51.
16. J. Kim: PhD Dissertation, 2012, Pohang University of Science and Technology, Pohang, South Korea.